

## **3.3 Strongly Correlated Quantum Systems**

# Tensor-Network Renormalization-Group Study of Critical Phenomena

Naoki KAWASHIMA

*Institute for Solid State Physics,*

*The University of Tokyo, Kashiwa-no-ha, Kashiwa, Chiba 277-8581*

We developed efficient methods, algorithms, parallelized programs, and sometimes new concepts, based on novel numerical techniques including the tensor network (TN) method and applied them to relevant physical problems. To list subjects of our research in 2021, (1) development of new numerical methods based on the TN representation [1,2], (2) study of TN ground states such as Kitaev spin liquid [3], (3) study of spin liquid in frustrated spin systems [4], (4) development of open-source applications [5].

In [1], we re-considered the method for extracting the critical information from the RSRG calculation with TNs. The most common method for obtaining the scaling dimension is to form a transfer matrix from the scale-invariant tensor. Then, we can obtain the scaling dimensions from its eigenvalues using the relationship derived from the conformal field theory. However, this method has not been generalized to three or higher dimensions. In our scheme, we construct a super-operator that represents the RSRG transformation. Without explicitly relying on the CFT, we derive the relationship between the eigenvalues of the super-

operator and the scaling dimensions. Our benchmark calculation on the 2D Ising model established validity of this basic idea. The new scheme may provide a direct method for estimating the scaling dimensions in higher dimensions.

In [2], we proposed a method for obtaining the excitation spectrum based on TN calculations. In this method, we consider an impurity tensor representing a locally excited state, and construct an eigenvalue equation in the space of such excited states, which can be block-diagonalized by Fourier transformation. By diagonalizing each block we can obtain excitation spectra of various excitations. We applied this scheme to one-dimensional quantum spin chain and successfully computed its excited states and the dynamical structure factor. We further investigated entanglement properties of excited states.

In [3], we considered in the Kitaev model on the honeycomb lattice and its extension to  $S=1$ . The models with arbitrary spin quantum numbers are not exactly solvable in contrast to the well-known Kitaev spin liquid solution of the spin-1/2 system. To unveil the important

difference between these states, we use the tensor-network wave functions, which proved, in our previous work, to be essential in capturing the nature of the Kitaev spin liquid. We found that the distinct sign structures of the tensor-network wave function for the integer- and half-integer-spin quantum spin liquids are responsible for completely different ground states in the spatially anisotropic limit.

In [4], we investigated  $S=1/2$  XXZ ladder system with four-spin interaction. The model can be viewed as a one-dimensional variant of the J-Q model on a square lattice. By means of variational uniform matrix product state (VUMPS) calculations and an effective field theory, we determine the phase diagram of the model and present evidence that the Néel-VBS transition is continuous and belongs to the Gaussian universality class with the central charge  $c=1$ . The full phase diagram consists of 8 distinct phases including magnetically ordered phases, Haldane-like phases, and VBS phases.

In [5], we developed DSQSS, an open-source software for quantum Monte Carlo simulation of lattice system. In [6], we applied it to the Bose-Hubbard model in the case of

extreme dilution to clarify the validity of the analytical predictions for the universal behavior of the model in this region. We confirmed the universal behaviors. In addition, we estimated model-dependent parameters such as the s-wave scattering length in a good agreement with the prediction as well as the non-universal correction term of the third order in the particle density, which has never been estimated before.

## References

- [1] X. Lyu, R. G. Xu and N. Kawashima, *Phys. Rev. Research* 3, 023048 (2021).
- [2] W.-L. Tu, H.-K. Wu, N. Schuch, N. Kawashima and J.-Y. Chen, *Phys. Rev. B* 103, 205155 (2021).
- [3] H.-Y. Lee, T. Suzuki, Y. B. Kim and N. Kawashima, *Phys. Rev. B* 104, 024417 (2021).
- [4] T. Ogino, S. Furukawa, R. Kaneko, S. Morita and N. Kawashima, *Phys. Rev. B* 104, 075135 (2021).
- [5] Y. Motoyama, K. Yoshimi, A. Masaki-Kato, T. Kato and N. Kawashima, *Comput. Phys. Commun.* 264, 107944 (2021).
- [6] A. Masaki-Kato, Y. Motoyama and N. Kawashima, *J. Phys. Soc. Jpn.* 90, 034711 (2022).

# Quantum Spin Liquids

Masatoshi IMADA

*Toyota Physical and Chemical Research Institute,  
41-1 Yokomichi, Nagakute, Aichi, 480-1192*

*and*

*Research Institute for Science and Engineering, Waseda University,  
3-4-1 Okubo, Shinjuku-ku, Tokyo, 169-8555*

## 1 Introduction

In this project, we have studied mechanisms of fractionalization in strongly correlated electron systems. One is the electron fractionalization, where an electron near the Mott insulator is splintered into a conventional quasiparticle and a dark fermion, which triggers the high temperature superconductivity in the copper oxide superconductors [1]. The second is the fractionalization of an electronic spin into spinons leading to quantum spin liquids.

Two types of quantum spin liquids were established by a high-accuracy quantum many-body solver that applies machine learning algorithm. In the quantum spin liquids, spin orientations are not ordered even at zero temperature. The first example is the case of  $J_1$ - $J_2$  Heisenberg model on the square lattice, where the geometrical frustration effect is crucial [3].

The other case is found in the Mott insulating phase of a molecular solid, in which the existence of the quantum spin liquid has been proposed for decades without clear understanding of its nature [4]. For the latter case, experimental results are reproduced with one-to-one correspondence by employing the first-principles methods based on real materials without adjustable parameters. In both cases, “spinon” emerging from the fractionalization of the ordinary spin excitation is suggested to be an elementary excitation, with gapless Dirac-type dispersion in the excitation

structure. They also share long-ranged quantum entanglement of spins and algebraic decay of spin correlation as common properties. However, there exists difference in that the isotropic 2D excitation in the  $J_1$ - $J_2$  Heisenberg model is contrasted with the strong 1D anisotropy in the molecular solid. These two typical examples offer a clue toward the understanding of the universality and diversity of the physics of quantum entanglement. In the present project, we also studied a possible spin liquid on a 3D pyrochlore lattice, which will be reported elsewhere. In this report, we focus on the *ab initio* study of quantum spin liquid in the molecular solid [4].

## 2 Quantum spin liquid in molecular solid

Molecular solids host various electronic phases. Especially,  $\beta'$ - $X$ [Pd(dmit)<sub>2</sub>]<sub>2</sub> with  $X$ =EtMe<sub>3</sub>Sb shows quantum spin-liquid (QSL) properties. We have studied five molecular-solid compounds with different  $X$  using 2D *ab initio* single-band effective Hamiltonian derived in Ref. [5, 6] in the form

$$\mathcal{H} = - \sum_{\sigma} \sum_{i,j} t_{ij} c_{i\sigma}^{\dagger} c_{j\sigma} + \sum_i U n_{i\uparrow} n_{i\downarrow} + \sum_{i<j} V_{ij} (n_i - 1)(n_j - 1), \quad (1)$$

where  $i, j$  represent the dimer indices, and  $c_{i\sigma}^{\dagger}$  ( $c_{i\sigma}$ ) is the creation (annihilation) opera-

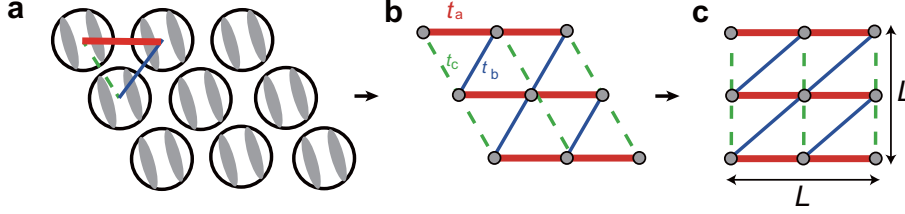


Figure 1: Lattice structure of  $\beta'$ - $X[\text{Pd}(\text{dmit})_2]_2$  [4]. **a**: Schematic triangular structure of  $\beta'$ - $X[\text{Pd}(\text{dmit})_2]_2$  consisting of dimerized  $\text{Pd}(\text{dmit})_2$  molecules, where a  $\text{Pd}(\text{dmit})_2$  molecule is depicted as a long gray oval. **b**: Modeled triangular lattice with three different electronic transfers. The strongest, middle and weakest transfers,  $t_a$  (on the red bond),  $t_b$  (on the blue bond), and  $t_c$  (on the green bond), respectively. **c**: Deformed structure on a  $L \times L$  lattice with the system size  $N_s = L^2$  used in the present calculation.

tor of electrons with spin  $\sigma$  ( $=\uparrow$  or  $\downarrow$ ) at the  $i$ -th Wannier orbital, and the number operator is  $n_i = \sum_{\sigma} n_{i\sigma}$  with  $n_{i\sigma} = c_{i\sigma}^{\dagger} c_{i\sigma}$ . Here,  $t_{ij}$  is the hopping parameters depending on the relative coordinate vector  $\mathbf{r}_i - \mathbf{r}_j$ , where  $\mathbf{r}_i$  is the position vector of the center of the  $i$ -th Wannier orbital. For  $t_{ij}$ , the nearest neighbor pair of  $\mathbf{r}_i$  and  $\mathbf{r}_j$  in each triangular direction is retained.  $U$  and  $V_{ij}$  are the screened on-site and off-site Coulomb interactions, respectively.  $V_{ij}$  is retained up to the third neighbor. The lattice structure we study is illustrated in Fig. 1. A variational Monte Carlo (VMC) method [7, 8, 9] is applied to the *ab initio* Hamiltonians to reach highly accurate ground states.

We have correctly reproduced experimental phase diagram with antiferromagnetic order for  $X=\text{Me}_4\text{P}$ ,  $\text{Me}_4\text{As}$ ,  $\text{Me}_4\text{Sb}$ ,  $\text{Et}_2\text{Me}_2\text{As}$  and a QSL for  $X=\text{EtMe}_3\text{Sb}$  without adjustable parameters [4]. as is shown in Fig. 2. It allows us to study the nature of the QSL at the microscopic level. The spin-spin correlations in real space  $C(\mathbf{r})$  for the QSL state of  $X=\text{EtMe}_3\text{Sb}$  indicates a power law  $C(\mathbf{r}) \propto |\mathbf{r}|^{-p}$  with  $p = 1.88 \pm 0.01$  in the strongest transfer direction suggesting the algebraic QSL with the gapless excitation. On the other hand, in the other directions,  $C(\mathbf{r}) \propto \exp[-|\mathbf{r}|/\xi_{\perp}]$  shows exponential decay with the correlation length  $\xi_{\perp} \sim 1.33 \pm 0.04$ . Therefore, the QSL for

$X=\text{EtMe}_3\text{Sb}$  exhibits 1D nature. It indicates a dimensional reduction from 2D to 1D. The 1D nature indeed accounts for the experimental specific heat, thermal conductivity and magnetic susceptibility. The identified QSL, however, preserves 2D nature as well consistently with spin fractionalization into spinon with Dirac-like gapless excitations and reveals duality bridging the 1D and 2D QSLs. The power  $p \sim 1.9$  is similar to the value obtained for the QSL in the square-lattice  $J_1$ - $J_2$  Heisenberg model with the nearest ( $J_1$ ) and the next-nearest-neighbor ( $J_2$ ) exchange interactions, where  $p \sim 1.4$ - $1.7$  [2]. However, in sharp contrast to isotropic 2D spin correlation in the  $J_1$ - $J_2$  model, the correlation decays exponentially in the interchain direction.

On the other hand, the signature of the 2D properties is also found in a prominent peak of the spin structure factor at  $(\pi, 0)$  and in the structure of the ground-state wave function itself [4]. In fact the excitation structure inferred from the wave-function form strongly supports the fractionalization of a spin into two spinons, similarly to the  $J_1$ - $J_2$  model [3]. The finding of the two types of QSL clarifies universal and system-dependent features of the QSL.

This is a combined report for E project 2020-Ea-0005 and 2020-Eb-0005 as well as shared project for Fugaku project. The present work was obtained by the collaboration with Kota

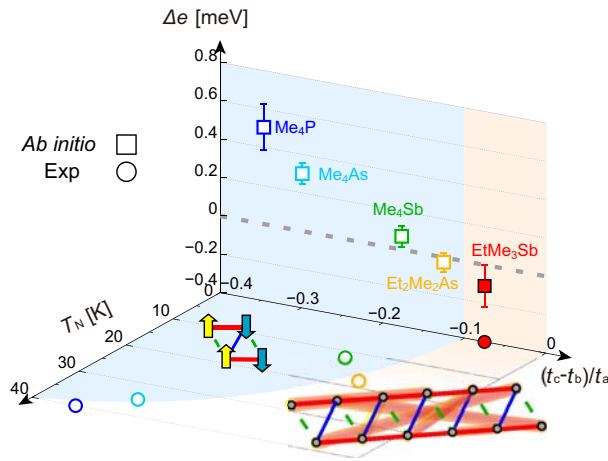


Figure 2: Ground-state phase diagram revealed by *ab initio* simulations (vertical plane), which shows agreement with the experimental phase diagram (bottom plane) [4].

Ido, Kazuyoshi Yoshimi and Takahiro Misawa. The work is also supported by JSPS Kakuenhi 16H06345, the RIKEN Center for Computational Science under the HPCI project (hp200132, hp210163, hp220166). The computation in this work has been done partially using the facilities of the Supercomputer Center, the Institute for Solid State Physics, the University of Tokyo. This project has used the software mVMC.

## References

- [1] M. Imada: J. Phys. Soc. Jpn. **90** (2021) 111009.
- [2] Y. Nomura and M. Imada: Phys. Rev. X **11** (2021) 031034.
- [3] Y. Nomura and M. Imada: Phys. Rev. X **11** (2021) 031034.
- [4] K. Ido, K. Yoshimi, T. Misawa and M. Imada: npj Quantum Materials: **7** (2022) 48.
- [5] K. Yoshimi, T. Misawa and T. Tsumuraya: Phys. Rev. Research **2**, (2020) 032072(R).
- [6] K. Yoshimi, T. Tsumuraya and T. Misawa: Phys. Rev. Research **3** (2021) 043224.
- [7] D. Tahara, and M. Imada: J. Phys. Soc. Jpn. **77** (2008) 114701.
- [8] T. Misawa *et al.* Comput. Phys. Commun. **235** (2019) 447.
- [9] Y. Nomura, A. S. Darmawan, Y. Yamaji and M. Imada: Phys. Rev. B **96** (2017) 205152.

# Numerical studies of Mott transitions in quantum spin liquid candidates

Youhei YAMAJI

*Center for Green Research on Energy and Environmental Materials,  
National Institute for Materials Science  
Namiki, Tsukuba-shi, Ibaraki 305-0044*

The Kitaev model is a unique solvable two-dimensional quantum system [1]. As shown by Kitaev, the ground state of the model hamiltonian is a quantum spin liquid. Later, Jackeli and Khaliullin proposed that the effective low-energy hamiltonian of Mott insulating phases of honeycomb iridium oxides such as  $\text{Na}_2\text{IrO}_3$  could be the Kitaev model [2]. Although the ground state of  $\text{Na}_2\text{IrO}_3$  was found to show a magnetic long-range order, the dominant terms in the *ab initio* effective spin hamiltonian of  $\text{Na}_2\text{IrO}_3$  are given by the Kitaev-type exchange couplings [3].

Even though there emerge new candidate materials represented by  $\alpha\text{-RuCl}_3$  on the front of the search for the spin-liquid ground states, an important question has not been solved yet: It has not been clarified yet whether the small Mott gaps of these candidate materials affect the properties of them or not. To elucidate an impact of the itinerant nature of electrons on the properties of a spin-liquid candidate, we studied the original *ab initio* itinerant hamiltonian consisting of iridium  $t_{2g}$  orbitals [3], instead of the spin hamiltonian.

In the present research, we studied the *ab initio*  $t_{2g}$  hamiltonian of  $\text{Na}_2\text{IrO}_3$  [3]. The  $t_{2g}$  hamiltonian consists of the kinetic energy and the intra-atomic and inter-atomic Coulomb repulsions as,

$$\hat{H}_{t_{2g}} = \hat{H}_K + \hat{H}_U + \hat{H}_V, \quad (1)$$

where  $\hat{H}_K$  represents the kinetic terms including trigonal distortion and spin-orbit cou-

plings,  $\hat{H}_U$  denotes the intra-atomic Coulomb interactions, and  $\hat{H}_V$  is the inter-atomic Coulomb repulsion.

Naïvely,  $\hat{H}_V$  is expected to be relevant to charge channels but irrelevant to spin degrees of freedom. However, it is not true. When inter-atomic exchange couplings are estimated by the second-order perturbation theory, the intra-atomic and intra-orbital Coulomb repulsion  $U$  in the energy denominator is replaced by  $U - V$ , where  $V$  is the inter-atomic Coulomb repulsion. Therefore, when the inter-atomic Coulomb repulsions are controlled as parameters, not only the charge but also the spin degrees of freedom are affected.

We controlled the nearest-neighbor, second nearest-neighbor, and  $1/r$  long-range Coulomb interactions to examine the competition among the magnetic and charge orders and suppression of the magnetic orders, by using an open-source code mVMC [4].

## References

- [1] A. Kitaev: Ann. Phys. (Amsterdam) **321** (2006) 2.
- [2] G. Jackeli and G. Khaliullin: Phys. Rev. Lett. **102** (2009) 017205.
- [3] Y. Yamaji, *et al.*: Phys. Rev. Lett. **113** (2014) 107201.
- [4] T. Misawa, *et al.*: Comput. Phys. Commun. **235** (2019) 447.

# Theoretical study of symmetry breaking and quantum transport phenomena in charge-spin-orbital coupled systems

Yukitoshi MOTOME

*Department of Applied Physics,*

*The University of Tokyo, Bunkyo, Tokyo 113-8656*

We have theoretically studied a variety of intriguing phenomena in correlated electron systems with charge-spin-orbital coupling (project numbers: 2021-Ca-0050 and 2021-Cb-0014). During the last fiscal year, we have achieved substantial progress on the following topics. We summarize the main results below.

(i) *Topological spin crystals*: Regarding topological spin crystals, such as skyrmion and hedgehog lattices, as moiré interferences between spin helices, we clarified how their magnetic and topological properties can be modulated by changing twist angles between the directions of the constituent spin density waves [1] and shifting relative phases [2,3,4]. We also elucidated charge modulation on such topological spin crystals [5]. In addition, we clarified the ground state phase diagrams [6] and spin excitations [7] for effective spin models with long-range interactions. We also clarified linear and nonlinear optical responses in quasi-one-dimensional chiral magnets [8,9]. We have collaborated with experimental groups [10,11]. We wrote a review article on the itinerant frustration mechanism [12].

(ii) *Kitaev quantum spin liquids*: We clarified

the effect of randomness on the spin dynamics in the Kitaev quantum spin liquid [13]. We also elucidated linear and nonlinear thermal transport in the presence of both uniform and staggered magnetic fields [14]. We have made collaborations with experimental groups on the topological nature in an external magnetic field [15,16]. In addition, we showed how to create and control fractional excitations by analyzing the effect of local lattice distortions [17]. We also proposed that iridium ilmenites can be good candidates for Kitaev magnets [18].

(iii) *Multipole physics*: We collaborated with experimental groups on a chiral magnet  $\text{Pb}(\text{TiO})\text{Cu}_4(\text{PO}_4)_4$  to clarify the control of magnetic domains [19] and nonreciprocal directional dichroism [20,21].

(iv) *Development of new theoretical methods*: We developed a many-body numerical method for quantum spin systems based on the Lefschetz thimbles technique [22]. We also developed new methods based on machine learning techniques: determinant-free fermionic wave function approach [23] and inverse design of Hamiltonians by using automatic differentiation [24].

## References

- [1] K. Shimizu, S. Okumura, Y. Kato, and Y. Motome, *Phys. Rev. B* **103**, 184421 (2021).
- [2] S. Hayami, T. Okubo, and Y. Motome, *Nat. Commun.* **12**, 6927 (2021).
- [3] K. Shimizu, S. Okumura, Y. Kato, and Y. Motome, preprint (arXiv:2201.03290).
- [4] K. Shimizu, S. Okumura, Y. Kato, and Y. Motome, *J. Phys.: Conf. Ser.* **2164** 012069 (2022).
- [5] S. Hayami and Y. Motome, *Phys. Rev. B* **104**, 144404 (2021).
- [6] Y. Kato and Y. Motome, preprint (arXiv:2202.04407).
- [7] Y. Kato, S. Hayami, and Y. Motome, *Phys. Rev. B* **104**, 224405 (2021).
- [8] S. Okumura, T. Morimoto, Y. Kato, and Y. Motome, *Phys. Rev. B* **104**, L180407 (2021).
- [9] S. Okumura, T. Morimoto, Y. Kato, and Y. Motome, *J. Phys.: Conf. Ser.* **2164** 012068 (2022).
- [10] K. Fujiwara, Y. Kato, T. Seki, K. Nomura, K. Takanashi, Y. Motome, and A. Tsukazaki, *Commun. Mater.* **2**, 113 (2021).
- [11] N. D. Khanh, T. Nakajima, S. Hayami, S. Gao, Y. Yamasaki, H. Sagayama, H. Nakao, R. Takagi, Y. Motome, Y. Tokura, T. Arima, and S. Seki, *Adv. Sci.* 2105452 (2022).
- [12] S. Hayami and Y. Motome, *J. Phys.: Condens. Matter* **33**, 443001 (2021).
- [13] J. Nasu and Y. Motome, *Phys. Rev. B* **104**, 045116 (2021).
- [14] K. Nakazawa, Y. Kato, and Y. Motome, preprint (arXiv:2201.04274), accepted for *Phys. Rev. B*.
- [15] T. Yokoi, S. Ma, Y. Kasahara, S. Kasahara, T. Shibauchi, N. Kurita, H. Tanaka, J. Nasu, Y. Motome, C. Hickey, S. Trebst, and Y. Matsuda, *Science* **373**, 568 (2021).
- [16] S. Suetsugu, Y. Ukai, M. Shimomura, M. Kamimura, T. Asaba, Y. Kasahara, N. Kurita, H. Tanaka, T. Shibauchi, J. Nasu, Y. Motome, and Y. Matsuda, preprint (arXiv:2203.00275).
- [17] S.-H. Jang, Y. Kato, and Y. Motome, *Phys. Rev. B* **104**, 085142 (2021)
- [18] S.-H. Jang and Y. Motome, *Phys. Rev. Materials* **5**, 104409 (2021).
- [19] K. Kimura, Y. Kato, S. Kimura, Y. Motome, and T. Kimura, *npj Quantum Mater.* **6**, 54 (2021).
- [20] T. Katsuyoshi, K. Kimura, Z. Yang, Y. Kato, S. Kimura, Y. Motome, Y. Kohama, and T. Kimura, *J. Phys. Soc. Jpn.* **90**, 123701 (2021).
- [21] M. Akaki, K. Kimura, Y. Kato, Y. Sawada, Y. Narumi, H. Ohta, T. Kimura, Y. Motome, and M. Hagiwara, *Phys. Rev. Research* **3**, L042043 (2021).
- [22] P. A. Mishchenko, Y. Kato, and Y. Motome, *Phys. Rev. D* **104**, 074517 (2021).
- [23] K. Inui, Y. Kato, and Y. Motome, *Phys. Rev. Research* **3**, 043126 (2021).
- [24] K. Inui and Y. Motome, preprint (arXiv:2203.07157).

# Low-energy excitations of skyrmion crystals in a centrosymmetric spin-charge coupled magnet

Masahito MOCHIZUKI

*Department of Applied Physics, Waseda University  
Okubo, Shinjuku-ku, Tokyo 169-8555*

In this project, we have theoretically studied the low-energy dynamics of skyrmion crystals in a centrosymmetric Kondo-lattice magnet with conduction-electron-mediated magnetic interactions (project ID: 2021-D-0002).

We computed the dynamical spin- and charge-structure factors of skyrmion crystals in a centrosymmetric spin-charge coupled magnet by taking the Kondo-lattice model with a classical treatment of localized spins. Our large-scale adiabatic molecular dynamics simulations revealed four Goldstone modes in the absence of an external magnetic field [Figure 1]. Three of the four Goldstone modes are associated with the spontaneous breaking of the  $SO(3)$  symmetry in spin space, and thus linearly dispersing. The remaining one is the so-called phonon mode associated with the displacement of skyrmions, and thus quadratically dispersing. Surprisingly, we observed clear segregation of spin and charge excitations: the three linearly dispersive Goldstone modes have full contribution from the spin sector and the quadratically dispersive Goldstone mode has full contribution from the charge sector [1]. Note that the dynamical structure factors obtained with the adiabatic molecular dynamics simulations perfectly coincide with the dispersion relations obtained with the linear-spin-wave calculation.

In our adiabatic molecular dynamics simulations, instead of repeated full diagonalizations of the quadratic form Hamiltonian, we utilized the kernel polynomial method in

combination with the automatic differentiation technique to evaluate the local physical quantities, for example, expectation values of itinerant electron spins and local charge occupations. The Chebyshev moments are evaluated using the combination of processing and threaded parallelization techniques on 18,432 cores (144 nodes) of System B Ohtaka.

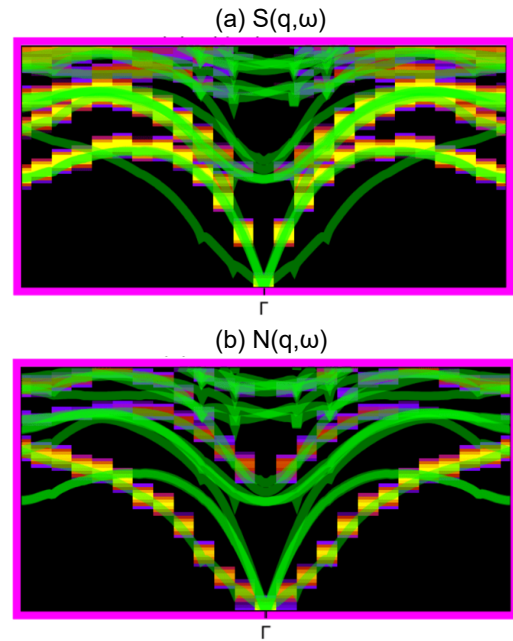


Figure 1: Dynamical (a) spin- and (b) charge-structure factors of the skyrmion crystal in the absence of an external magnetic field.

## References

- [1] R. Eto, R. Pohle, and M. Mochizuki, preprint [arXiv:2203.01496].

# Theoretical study on the photodriven spin and charge dynamics of topological materials

Masahito MOCHIZUKI

*Department of Applied Physics, Waseda University  
Okubo, Shinjuku-ku, Tokyo 169-8555*

We have theoretically studied the dynamics of topological magnetism and topological electron states under periodic driving (project ID: 2021-Ba-0015, 2021-Cb-0009). The main results of these projects are listed below.

- (i) *Dynamical magnetic topology switching of skyrmion crystals*: We revealed novel dynamics of skyrmion crystals in a centrosymmetric spin-charge coupled system under the microwave magnetic field [1]. By taking the Kondo-lattice model with a classical treatment of localized spins, we clarified the dynamic topological phase transitions of the skyrmion crystals among their skyrmion number  $N_{\text{sk}} = 2, 1,$  and  $0$  through the large-scale spin dynamics simulations in combination with the kernel polynomial method and the automatic differentiation technique. The topological phase transitions are induced by the effective magnetic field perpendicular to the rotating plane of the circularly polarized microwave magnetic field. In our numerical simulations with the kernel polynomial method and the automatic differentiation technique, we utilized our own hybrid parallelization code using both the processing parallelization with the message passing interface and the threaded parallelization with OpenMP. Moreover, in the automatic differentiation process, we reduced the computational cost for the evaluation of Chebyshev moments by using the relation  $2T_m(x)T_n(x) = T_{m+n}(x) + T_{|m-n|}(x)$  where  $T_m(x)$  denotes the  $m$ -th order first-kind Chebyshev polynomial.
- (ii) *Spin-wave eigenmodes of the quadruple- $Q$*

*magnetic hedgehog lattices in chiral magnets*: We studied the spin-wave eigenmodes of the quadruple- $Q$  hedgehog lattices which appear in the Kondo-lattice model on the cubic lattice by the spin-dynamics simulations in combination with the kernel polynomial method [2]. As a result, under the [001] magnetic field, we clarified two eigenmodes with counterclockwise fashion for the ac magnetic field perpendicular to [001] and four eigenmodes for the ac magnetic field parallel to [001]. Three of the four eigenmodes parallel to [001] are localized around point defects of magnetic textures, and the remaining one is closely related to the phase degrees of freedom.

(iii) *Photodriven dynamical phase transitions in the  $\alpha$ -type organic salt*: We clarified the dynamical phase transitions in the charge ordered organic salt  $\alpha$ -(BEDT-TTF) $_2$ I $_3$  under the irradiation of laser by the time-dependent mean-field calculation and the Floquet theory [3]. The sufficient intensity of laser melts the charge order and induces the semimetal phase. A much stronger laser induces the Chern insulator phase with nonzero Hall conductivity.

## References

- [1] R. Eto and M. Mochizuki, Phys. Rev. B **104**, 104425 (2021).
- [2] R. Eto and M. Mochizuki, in preparation.
- [3] Y. Tanaka and M. Mochizuki, preprint [arXiv:2203.04542].

# Topological phases, excitation modes, effects of exceptional points and transport phenomena in strongly correlated systems

Norio KAWAKAMI

*Department of Physics,*

*Kyoto University, Kitashirakawa, Sakyo-ku, Kyoto 606-8502*

Correlated materials have appeared as an arena to study non-Hermitian phenomena, such as exceptional points emerging in the single-particle Green's function. Exceptional points are degeneracies of eigenvalues due to the non-Hermiticity of a matrix. Contrary to Hermitian degeneracies, the eigenvalues and the eigenvectors coalesce at an exceptional point, giving rise to novel phenomena.

In [1], we show that topological Kondo insulators are an ideal platform for studying these phenomena due to a combination of strong correlations and surface states. Using numerical simulations, we demonstrate the emergence of exceptional points in the single-particle Green's function on the surface of the material while the bulk is still insulating. We believe that this situation is perfect for experimental observation of exceptional points. In particular, we reveal how quasiparticle states with long lifetimes are created on the surface by non-Hermitian effects while the Dirac cones are smeared. This effect is related to the surface Kondo breakdown at which heavy Dirac cones disappear from the single-particle spectrum and are replaced by light states.

Furthermore, we study nonlinear responses in strongly correlated systems, specifically analyzing the effect of renormalization and non-Hermiticity on the second-order nonlinear response.

Nonlinear responses in condensed matter are recently intensively studied because they provide rich information about the materials

and hold the possibility of being applied in diodes or high-frequency optical devices. While nonlinear responses in noninteracting models have been explored widely, the effect of strong correlations on the nonlinear response is still poorly understood. In [2], we first derive a formula for calculating the nonlinear response at finite temperatures that is entirely based on single-particle Green's functions. We furthermore analytically show that nonlinear responses are significantly enhanced by the renormalization of the band structure and non-Hermiticity in the Green's function. Finally, we confirm our analytical prediction by performing numerical calculations for several strongly correlated models.

In [3], we use this Green's function method to study the nonlinear Hall effect in  $\text{Ce}_3\text{Bi}_4\text{Pd}_3$ . Experiments measured a huge nonlinear Hall effect in this material. From symmetry analysis, we develop a model describing  $\text{Ce}_3\text{Bi}_4\text{Pd}_3$  as a Weyl-Kondo semimetal. Performing dynamical mean-field calculations for this model, we find that below the Kondo temperature, Weyl points emerge close to the Fermi energy in the band structure; at high temperatures, this material is a metal. Due to strong correlations, the band structure is strongly renormalized. We then directly calculate the nonlinear longitudinal conductivity and the nonlinear Hall conductivity and find that the nonlinear Hall resistivity is strongly enhanced compared to a noninteracting system. We find good agreement between our numerical calculations and the

experimental observations.

In [4], we analyze the effect of strong correlations on fragile topological insulators. Fragile topological insulators (FTIs) offer obstruction to the formation of exponentially localized Wannier functions, but they can be trivialized by adding certain trivial degrees of freedom. For the same reason, FTIs do not host symmetry-protected flow of edge states between bulk bands in cylindrical boundary conditions. Still, they are expected to have a spectral flow between the fragile bands and other bands under certain twisted boundary conditions. We analyze commonly observed effects of strong correlations, such as the Mott insulator transition and magnetism, on a known model hosting fragile topology. We show that fragile topology, along with the twisted boundary states, is stable with interactions below a critical interaction strength in the nonmagnetic case. Above this interaction strength, a transition to the Mott insulating phase occurs, and the twisted boundary states disappear. Furthermore, the fragile topology is destroyed by a homogeneous magnetic field. However, we show that a magnetic field can induce a topological phase transition which converts a fragile topological insulator to a Chern insulator. Finally, we study ferromagnetic solutions of the fragile topological model.

In [5], we investigate magnetic instabilities in charge-neutral twisted bilayer graphene close to so-called “magic angles” using a combination of real-space Hartree-Fock and dynamical mean-field theories. We find that localized magnetic states emerge for values of the Coulomb interaction  $U$  that are significantly smaller than what would be required to render an isolated layer antiferromagnetic. Our findings shed new light on perspectives for experimental realization of magnetic states in charge-neutral twisted bilayer graphene.

In [6], we analyze the impact of critical nematic fluctuations on the low energy properties of phonons. We propose how to identify the three-state Potts nematic fluctuations by ultrasound attenuation. The Landau damping term becomes isotropic due to fluctuations of the  $C_3$ -breaking bond-order, and the nemato-elastic coupling is also isotropic. The transverse sound attenuation coefficient diverges isotropically, in contrast to the case of the  $C_4$ -breaking bond-order that shows strong anisotropy. The shift of the first order transition line at low temperatures toward the second-order line renders the transition a weak first order in a wide range of parameters.

## References

- [1] R. Peters, K. Kimura, Y. Michishita, T. Yoshida, and N. Kawakami: “Surface exceptional points in a topological Kondo insulator” *Phys. Rev. B* **104** (2021) 235153.
- [2] Y. Michishita and R. Peters: “Effects of renormalization and non-Hermiticity on nonlinear responses in strongly-correlated electron systems” *Phys. Rev. B* **103** (2021) 195133.
- [3] A. Kofuji, Y. Michishita, and R. Peters: “Effects of strong correlations on the nonlinear response in Weyl-Kondo semimetals” *Phys. Rev. B* **104** (2021) 085151.
- [4] A. Joshi and R. Peters: “Mott transition and magnetism in a fragile topological insulator” *Phys. Rev. B* **103** (2021) 165130.
- [5] J. Vahedi, R. Peters, A. Missaoui, A. Honecker, and G. T. de Laissardière: “Magnetism of magic-angle twisted bilayer graphene” *SciPost Phys.* **11** (2021) 083.
- [6] K. Kimura, M. Sigrist, and N. Kawakami: “Probing three-state Potts nematic fluctuations by ultrasound attenuation” *Phys. Rev. B* **105** (2022) 035130.

# Finite-temperature methods for quantum many-body systems using Boltzmann machines

Yusuke NOMURA

*RIKEN Center for Emergent Matter Science, 2-1 Hirosawa, Wako, 351-0198*

The thermal behavior of many-body systems is a fundamental problem. Celebrated statistical mechanics provides a theoretical framework for describing finite-temperature properties. However, in quantum many-body systems, due to the "curse of dimensionality" of Hilbert space, it is very difficult to capture the complex competition between thermal and quantum fluctuations. Although various numerical methods have been developed, such as quantum Monte Carlo, diagrammatic, and tensor network methods, it is challenging to establish a reliable methodology that can be extended to the most exotic and interesting regions in quantum many-body physics.

Here, we take a novel approach using artificial neural networks. In particular, we employ deep Boltzmann machines that have flexible representability. We propose two different approaches, offering paths to encode many-body thermal physics into deep Boltzmann machines. In the first method, we find a completely deterministic way to construct deep Boltzmann machines that reproduce the exact purified expression of finite temperature states. In the second method, we

numerically optimize deep Boltzmann machines to reproduce imaginary time Hamiltonian evolution as accurately as possible within the representability of deep Boltzmann machines. We apply the methods to the transverse-field Ising model and the two-dimensional  $J_1$ - $J_2$  Heisenberg model. The numerical benchmarks show that our scalable approach can successfully simulate the finite-temperature properties of the quantum spin problems.

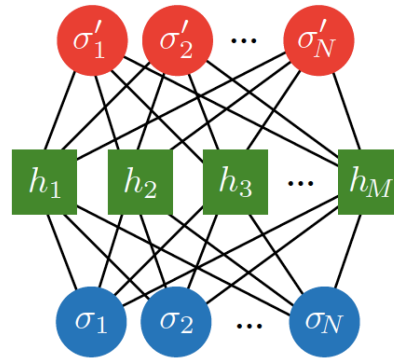


Fig. 1: Structure of deep Boltzmann machine employed in the present study.

## References

- [1] Y. Nomura, N. Yoshioka, and F. Nori, Phys. Rev. Lett. **127**, 060601 (2021)

# Exotic phenomena induced by strong correlations and non-Hermitian topology

Tsuneya Yoshida

*Department of Physics,*

*1-1-1 Tennodai, Tsukuba, Ibaraki, JAPAN 305-8571*

In this year, we have mainly studied non-Hermitian topological phenomena by focusing on exceptional points [1-4]. In particular, we have analyzed exceptional points at surfaces of topological Kondo insulators[1]. Specifically, we have applied the dynamical mean-field theory combined with the numerical renormalization group method to a variant of the periodic Anderson model which describes the topological Kondo insulator SmB6. Our numerical simulation has elucidated that finite lifetime of quasi-particles induces exceptional points at surfaces of the topological Kondo insulator. These exceptional points induce additional low energy excitations and change the spin structure of surface states (see Fig. 1).

We also have analyzed correlations effects on the non-Hermitian topology in zero dimension[4], where we have observed that the classification of the point-gap topology is reduced to  $Z_2$  while the classification is  $Z$  at the non-

interacting level.

Furthermore, we have explored the topological structure of the classical systems[5-7]. In particular, we have observed Hermitian and non-Hermitian topological physics in systems of the head conduction and the evolutionary game theory. The topological properties of superconductors are also discussed [8,9].

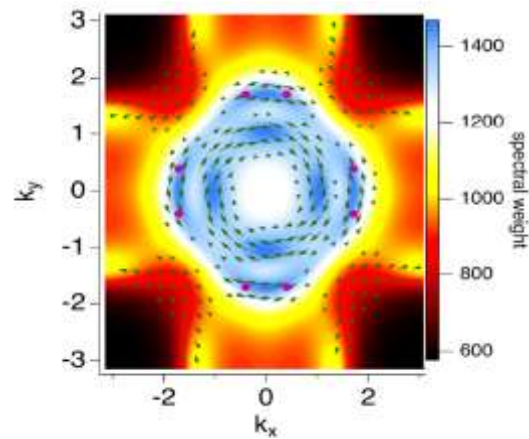


Fig.1 Spectral weight for a surface of a topological Kondo insulator. The emergence of exceptional points induces low energy excitations and affects the spin structure of the surface states (The figure is taken from Ref. [1])

## References

- [1] R. Peters, K. Kimura, Y. Michishita, T. Yoshida, and N. Kawakami, Phys. Rev. B **104** 235153 (2021).
- [2] T. Yoshida, R. Okugawa, and Y. Hatsugai, Phys. Rev. B **105**, 085109
- [3] H. Wakao, T. Yoshida, and Y. Hatsugai arXiv:2203.05773
- [4] T. Yoshida and Y. Hatsugai, Phys. Rev. B **104**, 075106 (2021).
- [5] T. Yoshida, T. Mizoguchi, and Y. Hatsugai, Phys. Rev. E **104**, 025003
- [6] S. Makino, T. Fukui, T. Yoshida, and Y. Hatsugai, Phys. Rev. E **105**, 024137 (2021)
- [7] T. Yoshida, T. Mizoguchi, and Y. Hatsugai, Sci. Rep. **12**, 1-7 (2021)
- [8] T. Yoshida, T. Mizoguchi, Y. Kuno, and Y. Hatsugai, Phys. Rev. B **103**, 235130 (2021)
- [9] Y. Yanase, A. Daido, K. Takasan, and T. Yoshida, Physica E, **140**, 115143 (2022)

# Extreme response of isotropic spin fluctuations emerging from anisotropic antiferromagnets under moderate spin dilution

Hidemaro SUWA

*Department of Physics, University of Tokyo, Tokyo 113-0033*

The stability and response of magnetic materials to external stimuli are determined by spin fluctuations dictated by magnetic anisotropy. The two-dimensional (2D) isotropic antiferromagnet is one of the ideal cases to pursue an extreme magnetic response. However, magnetic anisotropy is significant in most materials, reducing the magnetic response. As a perturbation, magnetic anisotropy introduces a characteristic length scale  $\xi_{\text{ani}}$ . The significance of anisotropy follows from the fact that the correlation length increases rapidly with decreasing temperature and easily reaches  $\xi_{\text{ani}}$ . In contrast, the Zeeman energy from a typical achievable magnetic field is weaker, and the length scale  $\xi_{\text{ext}}$  introduced by the external field is much larger, i.e.,  $\xi_{\text{ext}} > \xi_{\text{ani}}$ . Moreover, the Zeeman field in antiferromagnets must be a staggered field that is linearly coupled to the staggered magnetization, which is difficult to realize.

Our primitive 2D antiferromagnet is realized on a pseudo spin-1/2 square lattice embedded in a  $[(\text{SrIrO}_3)_1/(\text{SrTiO}_3)_2]$  superlattice, with the adjacent  $\text{IrO}_2$  planes well separated by non-magnetic spacers. Strong spin-orbit coupling of iridium stabilizes the  $J_{\text{eff}} = 1/2$  moment antiferromagnetically coupled to each other via the Heisenberg super-exchange interaction. An essential feature of such a  $J_{\text{eff}} = 1/2$  square lattice is that the large Dzyaloshinskii–Moriya interaction arising from the staggered rotation of the  $\text{IrO}_6$  octahedron around the  $c$  axis is canceled throughout the

lattice, and the pseudospins tend to be almost completely isotropic, which is called a hidden  $\text{SU}(2)$  symmetry. This phenomenon allows the in-plane uniform magnetic field to act as an effective staggered field. Nevertheless, higher-order super-exchange paths due to Hund’s coupling cause small easy-plane anisotropy, effectively reducing the spin symmetry from  $\text{SU}(2)$  to  $\text{U}(1)$ .

We have theoretically and experimentally demonstrated that we can switch the order of  $\xi_{\text{ext}}$  and  $\xi_{\text{ani}}$  utilizing magnetic dilution. Using ISSP System B in class C projects (ID: 2021-Ca-0117) and the ALPS/looper (<http://github.com/wistaria/alps-looper>) code, we simulated large-scale 2D AFM systems of more than one million quantum spins. We calculated the Berezinskii–Kosterlitz–Thouless transition temperatures for several dilution fractions. Using the crossover argument with multiple perturbations, we have shown that the response to magnetic fields changes from the  $\text{U}(1)$  model to the  $\text{SU}(2)$  model above the threshold dilution fraction because of the length-scale switch ( $\xi_{\text{ext}} < \xi_{\text{ani}}$ ). The theoretical calculation successfully accounts for the experimental observations, confirming the extreme response of isotropic fluctuations emerging from anisotropic antiferromagnets under moderate spin dilution.

# Research of Multi-Channel Kondo Effect Emerging from Heavy Rare-Earth Ions

Takashi HOTTA

*Department of Physics, Tokyo Metropolitan University  
1-1 Minami-Osawa, Hachioji, Tokyo 192-0397*

We have discovered the three-channel Kondo effect in the cubic Ho compound [1]. We have analyzed a seven-orbital impurity Anderson model hybridized with  $\Gamma_8$  and  $\Gamma_7$  conduction electrons for a case with ten local  $f$  electrons corresponding to a  $\text{Ho}^{3+}$  ion by using a numerical renormalization group (NRG) method. Then, we have found a residual entropy of  $\log \phi$  with the golden ratio  $\phi = (1 + \sqrt{5})/2$  as a signal of the three-channel Kondo effect for the local  $\Gamma_5$  triplet ground state.

For the construction of the local  $f$ -electron Hamiltonian  $H_{\text{loc}}$ , we introduce one  $f$ -electron state, defined by the eigenstate of spin-orbit and crystalline electric field (CEF) potential terms. Under the cubic CEF potential, we obtain  $\Gamma_7$  doublet and  $\Gamma_8$  quartet from  $j = 5/2$  sextet, whereas we find  $\Gamma_6$  doublet,  $\Gamma_7$  doublet, and  $\Gamma_8$  quartet from  $j = 7/2$  octet. By using those one-electron states as bases, we obtain  $H_{\text{loc}}$  as

$$\begin{aligned} H_{\text{loc}} = & \sum_{j,\mu,\tau} (\lambda_j + B_{j,\mu}) f_{j\mu\tau}^\dagger f_{j\mu\tau} + nE_f \\ & + \sum_{j_1 \sim j_4} \sum_{\mu_1 \sim \mu_4} \sum_{\tau_1 \sim \tau_4} I_{\mu_1 \tau_1 \mu_2 \tau_2, \mu_3 \tau_3 \mu_4 \tau_4}^{j_1 j_2, j_3 j_4} \quad (1) \\ & \times f_{j_1 \mu_1 \tau_1}^\dagger f_{j_2 \mu_2 \tau_2}^\dagger f_{j_3 \mu_3 \tau_3} f_{j_4 \mu_4 \tau_4}, \end{aligned}$$

where  $f_{j\mu\tau}$  is the annihilation operator of a localized  $f$  electron in the bases of  $(j, \mu, \tau)$ ,  $j$  is the total angular momentum,  $j = 5/2$  and  $7/2$  are denoted by “ $a$ ” and “ $b$ ”, respectively,  $\mu$  distinguishes the cubic irreducible representation,  $\Gamma_8$  states are distinguished by  $\mu = \alpha$  and  $\beta$ , while the  $\Gamma_7$  and  $\Gamma_6$  states are labeled by  $\mu = \gamma$  and  $\delta$ , respectively,  $\tau$  denotes the

pseudo-spin, which distinguishes the degeneracy concerning the time-reversal symmetry,  $n$  is the local  $f$ -electron number at an impurity site, and  $E_f$  is the  $f$ -electron level to control  $n$ . Here we set  $\hbar = k_B = 1$  and the energy unit as eV.

Concerning the spin-orbit term, we obtain  $\lambda_a = -2\lambda$  and  $\lambda_b = (3/2)\lambda$ , where  $\lambda$  is the spin-orbit coupling of  $f$  electron. In this study, we set  $\lambda = 0.265$  for the Ho ions. Concerning the CEF potential term for  $j = 5/2$ , we obtain  $B_{a,\alpha} = B_{a,\beta} = 1320B_4^0/7$  and  $B_{a,\gamma} = -2640B_4^0/7$ , where  $B_4^0$  denotes the fourth-order CEF parameter for the angular momentum  $\ell = 3$ . For  $j = 7/2$ , we obtain  $B_{b,\alpha} = B_{b,\beta} = 360B_4^0/7 + 2880B_6^0$ ,  $B_{b,\gamma} = -3240B_4^0/7 - 2160B_6^0$ , and  $B_{b,\delta} = 360B_4^0 - 3600B_6^0/7$ . In the present calculations, we treat  $B_4^0$  and  $B_6^0$  as parameters. For the Coulomb interaction terms, we do not show the explicit forms of  $I$  here, but they are expressed by the four Slater-Condon parameters,  $F^0$ ,  $F^2$ ,  $F^4$ , and  $F^6$ . These values should be determined from experimental results, but here we simply set the ratio as  $F^0/10 = F^2/5 = F^4/3 = F^6 = U$ , where  $U$  indicates the Hund’s rule interaction among the  $f$  orbitals and the magnitude is set as unity in this study.

In Fig. 1, we show the local CEF ground-state phase diagram for  $n = 10$ . The ground-state multiplet for  $B_4^0 = B_6^0 = 0$  is characterized by the total angular momentum  $J = 8$ . Under the cubic CEF potentials, the sept-

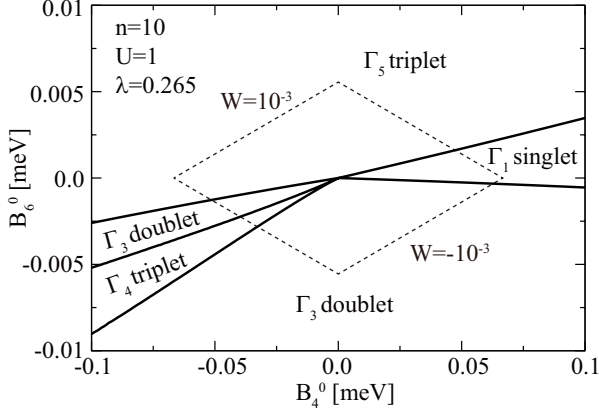


Figure 1: Local CEF ground-state phase diagram on the  $(B_4^0, B_6^0)$  plane for  $n = 10$  with  $U = 1$  and  $\lambda = 0.265$ .

dectet of  $J = 8$  is split into four groups as one  $\Gamma_1$  singlet, two  $\Gamma_3$  doublets, two  $\Gamma_4$  triplets, and two  $\Gamma_5$  triplets. Then, we obtain four kinds of local ground states for  $n = 10$ , as shown in Fig. 1. The dashed rhombus denotes the trajectory of  $B_4^0 = Wx/15$  and  $B_6^0 = W(1 - |x|)/180$  for  $-1 \leq x \leq 1$  with  $W = \pm 10^{-3}$ . Roughly speaking, the  $\Gamma_5$  triplet appears widely for  $B_6^0 > 0$ , whereas the  $\Gamma_3$  doublet is found for  $B_6^0 < 0$ . In the region of  $B_6^0 \approx 0$  and  $B_4^0 > 0$ , the  $\Gamma_1$  singlet was stabilized. For  $B_4^0 < 0$ , we find the  $\Gamma_3$  doublet and  $\Gamma_4$  triplet in a narrow region between the  $\Gamma_5$  triplet and  $\Gamma_3$  doublet.

Now we include the  $\Gamma_7$  and  $\Gamma_8$  conduction electron bands. Here we consider only the hybridization between the conduction and  $j = 7/2$  electrons. The Hamiltonian is given by

$$H = \sum_{\mathbf{k}, \mu, \tau} \varepsilon_{\mathbf{k}} c_{\mathbf{k}\mu\tau}^\dagger c_{\mathbf{k}\mu\tau} + \sum_{\mathbf{k}, \mu, \tau} V_\mu (c_{\mathbf{k}\mu\tau}^\dagger f_{b\gamma\tau} + \text{h.c.}) + H_{\text{loc}}, \quad (2)$$

where  $\varepsilon_{\mathbf{k}}$  is the dispersion of conduction electron with wave vector  $\mathbf{k}$ ,  $c_{\mathbf{k}\gamma\tau}$  is an annihilation operator of conduction electrons, and  $V_\mu$  denotes the hybridization between  $f$  electron in the  $\mu$  orbital and conduction electron of the  $\mu$  band. Here we set  $V_\alpha = V_\beta = V_\gamma = V$ .

In this research, we analyze the model by employing the NRG method [2]. We introduce

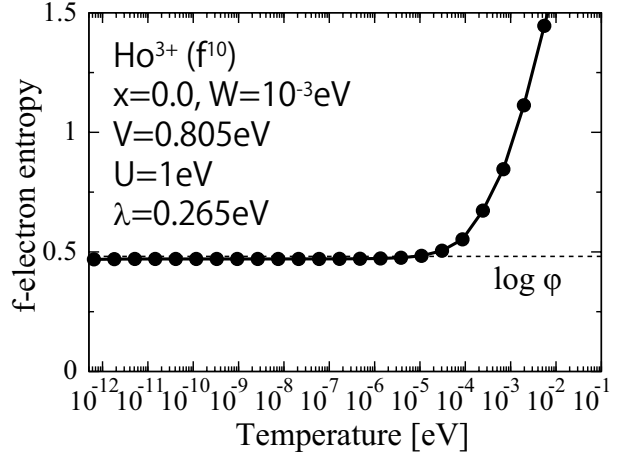


Figure 2: Entropy vs. temperature for  $n = 10$  with  $x = 0.0$  and  $W = 10^{-3}$ , corresponding to the  $\Gamma_5$  triplet ground state.

a cut-off  $\Lambda$  for the logarithmic discretization of the conduction band. Due to the limitation of computer resources, we keep  $M$  low-energy states. Here we use  $\Lambda = 8$  and  $M = 5,000$ . In the NRG calculation, the temperature  $T$  is defined as  $T = D\Lambda^{-(N-1)/2}$ , where  $D$  is half the conduction band width, which was set as 1 eV, and  $N$  is the number of renormalization steps.

Here we briefly discuss the typical result for  $n = 10$  [1]. In Fig. 2, we show entropy vs. temperature for the  $\Gamma_5$  triplet ground state. We observe a residual entropy of  $\log \phi$  at low temperatures with the golden ratio  $\phi = (1 + \sqrt{5})/2$ , which is characteristic of the three-channel Kondo effect. We confirm the residual entropy of  $\log \phi$  in the wide region of the local  $\Gamma_5$  triplet ground state. Thus, we conclude that the three-channel Kondo effect occurs in the  $\Gamma_5$  triplet ground state of  $\text{Ho}^{3+}$  ions.

## References

- [1] T. Hotta, J. Phys. Soc. Jpn. **90**, 113701 (2021).
- [2] H. R. Krishna-murthy, J. W. Wilkins, and K. G. Wilson, Phys. Rev. B **21**, 1003 (1980).

# Numerical study of topological thermal transport in Kitaev-related systems

Joji NASU

*Department of Physics, Tohoku University  
Sendai 980-8578*

The Kitaev quantum spin model has been intensively investigated since the proposal by A. Kitaev as a canonical model exhibiting quantum spin liquids. This model is considered to describe the magnetism of iridium oxides and  $\alpha$ -RuCl<sub>3</sub> where the strong spin-orbit coupling and electron correlations are present. However, these materials show a magnetic order at low temperatures due to magnetic interactions additional to the Kitaev term. As additional terms, effects of the Heisenberg interaction and off-diagonal symmetric term ( $\Gamma$  term) have been examined intensively. Moreover, recent experiments in  $\alpha$ -RuCl<sub>3</sub> clarified that an applied magnetic field induces nonzero thermal Hall conductivity, whose sign depends on the magnetic field direction. However, the field-angle dependence of the Kitaev-Heisenberg and Kitaev-Heisenberg- $\Gamma$  models remains unclear in the presence of magnetic orders.

In this project, we systematically examine the field-angle dependence of magnetic orders and excitation spectra in these models. To address the case with arbitrary spin directions in a magnetic order, we have newly developed the calculation technique by extending the conventional spin-wave theory [1, 2]. In this method, we can implement large-sublattice calculations straightforwardly. Our spin-wave theory needs the Cholesky decomposition. We use the LAPACK library to perform it. First, we examine the ground-state spin configuration by changing the magnetic field direction and obtain the phase diagram. Based on the ob-

tained ground-state magnetic orders, we calculate the energy and Berry curvature of the magnon bands. Furthermore, we calculate the temperature dependence of the thermal Hall conductivity. To compute the thermal Hall coefficient, we need to sum up the Berry curvature for the wave-number vector in the Brillouin zone. We parallelize the  $k$ -summation in the ISSP supercomputer to perform this procedure efficiently. The thermal Hall conductivity is enhanced in magnetically ordered states with noncoplanar spin configurations. Moreover, we also find that the thermal Hall effect originating from the topological nature of the magnon dispersion is absent when the field is applied along with one of the spin axes in the Kitaev-Heisenberg model. We also find that this feature disappears by introducing the off-diagonal symmetric  $\Gamma$  interaction. In addition, we clarify that the  $\Gamma$  interaction suppresses the thermal Hall conductivity because of enhancing the low-energy magnon gap.

## References

- [1] S. Koyama and J. Nasu: B **104** (2021) 075121.
- [2] S. Koyama and J. Nasu: J. Phys.: Conf. Ser. **2164** (2022) 012071.

# Searching for meron crystal in itinerant magnets

Satoru Hayami

*Department of Applied Physics, The University of Tokyo, Tokyo 113-8656*

Topological spin textures, such as a magnetic skyrmion, meron, and hedgehog, have attracted considerable attention, since they give rise to fascinating physical phenomena, such as the topological Hall effect. The fundamental understanding of the stabilization mechanisms for these nontrivial spin textures would be useful for potential applications to next-generation electronic and spintronic devices. In the project with number 2021-Ca-0042, we have theoretically investigated the possibility of such topological spin textures based on an itinerant electron model and its effective spin model. We have presented the main results this year below.

*(i) Skyrmion crystals in trigonal systems:* We have theoretically investigated a new stabilization mechanism of the skyrmion crystals in itinerant trigonal systems [1]. By focusing on the anisotropic exchange interaction that originates from the lack of horizontal mirror symmetry and twofold rotational symmetry along the threefold axis, we obtained two types of skyrmion crystals with the skyrmion number of one and two. We have shown that two SkXs are transformed with each other by changing the magnetic field. Our findings suggest itinerant trigonal systems as a new skyrmion-hosting system in addition to conventional hexagonal and tetragonal systems.

*(ii) Mechanism of skyrmion crystals in EuPtSi:* We have theoretically studied the stabilization mechanism of the skyrmion crystals in the  $f$ -electron compound EuPtSi based on an effective spin model [2]. We found two important ingredients to induce the skyrmion crystal: (1) the multiple- $q$  superpositions of

the spirals with low-symmetric ordering vectors and (2) the synergy between spin-charge and spin-orbit couplings in itinerant magnets. We have clarified that the model to satisfy two conditions well describes the skyrmion physics in EuPtSi by performing unbiased simulated annealing.

*(iii) Meron-antimeron crystal on a triangular lattice:* A meron-antimeron crystal consisting of the periodic array of merons and antimerons with a half skyrmion number has attracted growing attention since its observation in  $\text{Co}_8\text{Zn}_9\text{Mn}_3$  and  $\text{Gd}_2\text{PdSi}_3$ . Nevertheless, its origin has not been fully identified owing to the lack of a stabilization mechanism and an appropriate model. To understand the origin of the meron-antimeron crystals on the basis of metallic magnets, we theoretically performed simulated annealing for an effective spin model derived from the Kondo lattice model on a noncentrosymmetric triangular lattice [3]. As a result, we showed that several types of meron-antimeron crystals are stabilized by the synergy among the biquadratic interaction, the single-ion anisotropy, and the Dzyaloshinskii-Moriya interaction. The emergent meron-antimeron crystals are owing to the nature of itinerant electrons, which have not been obtained in localized spin models. We also found other topological spin textures including the skyrmion crystal can be realized by the same effective model at zero fields.

*(iv) Charge density waves in multiple- $Q$  spin states:* We elucidated the charge density wave formation in the presence of the spin density wave [4]. Based on the perturbation in terms of the spin-charge coupling, we theoretically

derived a useful formula for the relationship between charge density waves and spin density waves, which can be applied to any type of magnetic texture and lattice structure. We have tested the obtained formula for several single- $Q$  and double- $Q$  magnetic orderings including the skyrmion crystal on a square lattice. We have also shown the effects of large spin-charge coupling beyond the perturbative regime and the spin-orbit coupling to comprehensively understand the charge density wave formation in itinerant magnets.

*(v) Phase shift in skyrmion crystals:* We have theoretically studied the possibility of controlling the skyrmion crystals by using the phase degree of freedom among the spin density waves [5]. We have shown that a phase shift can occur in the skyrmion crystals to stabilize a new type of vortex crystals with a different pattern of an emergent magnetoelectric field through local scalar spin chirality, which gives rise to nonreciprocal transport phenomena without the spin-orbit coupling. Analyzing the Kondo lattice model and its effective spin model, we found three mechanisms to cause the phase shift: exchange interactions between the localized spins, thermal fluctuations, and long-range chirality interactions.

*(vi) Skyrmion crystal in centrosymmetric bilayer magnets:* We proposed a stabilization mechanism to realize the skyrmion crystal in centrosymmetric bilayer magnets [6]. By performing the simulated annealing on the bilayer triangular-lattice spin model, we have shown that the interplay between the layer-dependent Dzyaloshinskii-Moriya interaction and interlayer exchange interaction gives rise to the skyrmion crystal even without the frustrated exchange interaction and multiple-spin interactions. In addition, we have obtained two triple- $Q$  states with a uniform scalar chirality while increasing and decreasing the magnetic field in the skyrmion crystal phase that has not been obtained in the single-layer system.

*(vii) Multiple skyrmion crystals in tetrag-*

*onal magnets:* We theoretically investigated the possibility of realizing multiple skyrmion crystals against an external magnetic field in tetragonal itinerant magnets [7]. By focusing on multiple peaks at bare susceptibility of itinerant electrons, we found that three types of skyrmion crystals with the skyrmion numbers of one and two, which are characterized by different superpositions of helices, are stabilized in the ground state. Moreover, we found that they are transformed with each other by an external magnetic field.

## References

- [1] R. Yambe and S. Hayami, *Sci. Rep.* **11**, 11184 (2021)
- [2] S. Hayami and R. Yambe, *J. Phys. Soc. Jpn.* **90**, 073705 (2021).
- [3] S. Hayami and R. Yambe, *Phys. Rev. B* **104**, 094425 (2021).
- [4] S. Hayami and Y. Motome, *Phys. Rev. B* **104**, 144404 (2021).
- [5] S. Hayami, T. Okubo, and Y. Motome, *Nat. Commun.* **12**, 6927 (2021).
- [6] S. Hayami, *Phys. Rev. B* **105**, 014408 (2022).
- [7] S. Hayami, *J. Phys. Soc. Jpn.* **91**, 023705 (2022).

# Analysis of string excitations in the optical conductivity of doped Mott insulators

Takami TOHYAMA

*Department of Applied Physics, Tokyo University of Science, Tokyo 125-8585*

The optical conductivity has provided important information on the nature of the hole-doped Mott insulators. The most striking feature is dynamical spectral-weight transfer upon chemical doping and photodoping appearing at mid-infrared (MIR) region. The weights at MIR are sensitive to dimensionality and are found in two dimensions but not in one dimension. MIR weights are expected to contain essential information on the dynamical properties of holes in the two-dimensional Mott insulators. A hole moving in antiferromagnetic (AFM) spin background creates misarranged spins with respect to their sublattice and consequently induces string-type excitation of spins. MIR weights may have a relation to string structures. However, it is unclear how MIR weights actually are related to string excitations that are the result of a complex process due to spin-charge coupling. If a hole moves in an AFM state, it leaves traces of spin mismatches with sublattice magnetization called  $S_z$  strings. The  $S_z$  strings are inadequate to describe a hole surrounded by AFM spins since the hole picks up a nontrivial  $U(1)$  phase when it hops in an AFM spin background. This phase generates another type of strings, called phase strings, caused by transverse spin component.

In this project, we demonstrate how much  $S_z$  and phase strings contribute to MIR weights. We calculate the optical conductivity of the Hubbard model in the strong-coupling regime and the  $t$ - $J$  model by using time-dependent Lanczos and

time-dependent density-matrix renormalization group (tDMRG) methods. We focus on doped Mott insulators with a single hole and consider two-leg ladders up to a  $20 \times 2$  sites [1] and square lattice up to  $6 \times 6$  sites [2] under open boundary conditions. Turning on and off the effect of phase strings, we examine how they contribute to MIR weights. We find that phase strings play an essential role in MIR weights. MIR weights are crucially suppressed for both the Hubbard and  $t$ - $J$  models if we remove phase strings. Although  $S_z$  strings also contribute to MIR weights, their contribution is smaller than phase strings. We consider that this is because  $S_z$  strings can be self-healed via quantum spin flips, while phase strings are not repairable. Our findings suggest that a mutual Chern-Simons gauge field, which is an elementary force between spin and charge in the phase-string theory, is significant for obtaining MIR weights. This indicates that a hole does not pick up a  $U(1)$  phase when moving in AFM spin background if we remove this gauge field. As a result, we can characterize a doped hole surrounded by AFM spins via a spin-polaron quasiparticle, which has a cosinelike energy dispersion in the single-particle spectral function.

## References

- [1] K. Shinjo, S. Sota, and T. Tohyama: Phys. Rev. B **103** (2021) 035141.
- [2] K. Shinjo, S. Sota, and T. Tohyama: in preparation.

# Theoretical Calculation on Coulomb Repulsion of EDXT Oligomer Charge Transfer Salts

Tomoko FUJINO

*Institute for Solid State Physics,*

*The University of Tokyo, Kashiwa-no-ha, Kashiwa, Chiba 277-8581*

We have synthesized discrete oligomer models for doped poly(3,4-ethylenedioxythiophene) (PEDOT) [1,2]. Doped PEDOT is a commonly employed conductive polymer in organic electronic devices owing to their flexibility, lightness, transparency, and concise synthetic routes. However, their complicated packing structures based on a non-uniform molecular weight distribution severely limit structural data acquisition, especially electronic structural data, requisite for further improving the physical properties.

This study calculated the band structures based on the single-crystal structures of charge transfer salts of the dimer as the shortest models for doped PEDOT [1]. The band calculations functional theory (DFT)-based by OpenMX software revealed their one-dimensional (1D) metallic band structures with a strong intracolumnar orbital interaction (calculated band width  $W \approx 1$  eV). This interaction was significantly stronger than that observed for

typical low molecular weight 1D conductors (TTF•TCNQ:  $4t_{\text{TTF}} \approx 0.2\text{--}0.4$  eV,  $4t_{\text{TCNQ}} \approx 0.5$  eV), revealing the origin of the high conductivity of doped PEDOT. Interestingly, the elongation of characteristic oligomer length from dimer to trimer exhibited decreased  $W$  ( $\approx 0.90$  eV), while it improved the conductivity with 70% activation energy (0.20 eV) of that for dimer. These data indicated that extending the conjugation lengths of the oligomers markedly lowered effective Coulomb repulsion ( $U_{\text{eff}}$ ), thereby decreasing the ratio of  $U_{\text{eff}}/W$  and improving the conductivity [2]. The details on  $U_{\text{eff}}$  by theoretical calculations will be discussed in near future.

## References

- [1]. R. Kameyama, T. Fujino, S. Dekura, M. Kawamura, T. Ozaki, and H. Mori: Chem. Eur. J. **27** (2021) 6696.
- [2] R. Kameyama, T. Fujino, S. Dekura, and H. Mori: Phys. Chem. Chem. Phys. **24** (2022), 9130.

# Studies of the superconductivity and magnetic states in the strongly correlated electron systems based on Hubbard models.

Atsushi Yamada

*Department of Physics, Chiba University*

*Chiba 263-8522, Japana, Chiba 277-8581*

A spin liquid state, which is a purely nonmagnetic Mott insulator without spontaneously broken spatial or spin symmetry, has attracted a lot of interest. This state is realized in geometrically frustrated systems like the charge organic transfer salts  $\kappa$ -(BEDT-TTF)<sub>2</sub>X[1] and Cs<sub>2</sub>CuCl<sub>4</sub>. [2]

A spin liquid could arise also in the intermediate coupling region of strongly correlated systems between a semi-metal and ordered state, because in this case a correlation-driven insulating gap might open before the system becomes ordered. This possibility might be realized in the half-filled Hubbard model on the honeycomb lattice, where a semi-metal is realized at  $U = 0$ , and in fact is studied, for example, using Quantum Monte Carlo (QMC) simulations. Meng *et al*[3] found that a spin liquid state is realized in the Honeycomb lattice Hubbard model. But subsequent QMC studies[4] with larger lattice size ruled out this possibility.

We have studied the magnetic and metal-to-insulator transitions by variational cluster approximation using 10-site and 16-site clusters as a reference system. Parts of numerical calculations were done using the computer facilities of the ISSP. We found that  $U_{AF} = 2.7$  and  $U_{MI} = 3.0$  for 10-site cluster, and  $U_{AF} = 2.7$  and  $U_{MI} = 3.2$  for 16-site cluster.[5] This result also rules out the existence of the spin liquid in this model. Our results agree with recent large scale Quantum Monte Carlo simulations.[4] To

study larger systems, we need to revise our program using MPI technique. We are now improving our programs, even though we encounter a lot of difficulties.

## References

- [1] Y. Shimizu, K. Miyagawa, K. Kanoda, M. Maesato, and G. Saito, Phys. Rev. Lett. **91**, 107001 (2003); Y. Kurosaki, Y. Shimizu, K. Miyagawa, K. Kanoda, and G. Saito, Phys. Rev. Lett. **95**, 177001 (2005).
- [2] R. Coldea, D.A. Tennant, A.M. Tsvelik, and Z. Tylczynski, Phys. Rev. Lett. **86**, 1335 (2001); R. Coldea, D.A. Tennant, and Z. Tylczynski, Phys. Rev. Lett. **68**, 134424 (2003).
- [3] Z. Y. Meng et al., Nature 464, 08942 (2010).
- [4] S. Sorella, Y. Otsuka, and S. Yunoki, Sci. Rep. **2**, 992 (2012); F. F. Assaad and I. F. Herbut, Phys. Rev. X **3**, 031010 (2013); F. Parisen Toldin, M. Hohenadler, F. F. Assaad, and I. F. Herbut, Phys. Rev. B **91**, 165108 (2015).
- [5] A. Yamada, Int. J. Mod. Phys. B **30**, 1650158 (2016).

# Non-Abelian anyons trapped in vacancies of the Kitaev model and non-local spin correlations

Masahiro O. TAKAHASHI and Satoshi FUJIMOTO

*Department of Materials Engineering Science, Osaka University  
Machikaneyama 1-3, Toyonaka, Osaka 560-8531*

We have clarified, using massive parallel computer simulations, that a non-local spin-spin correlation exists between specific spatially well-separated sites in the Kitaev spin liquid with some point vacancies, which reveals the realization of Majorana zero modes (MZMs) strongly trapped in vacancies.

The Kitaev model [1] is a spin-1/2 model defined with bond-dependent Ising interactions on the honeycomb lattice and it is exactly solvable with the use of an itinerant Majorana fermion and a  $Z_2$  flux defined on each plaquette. In a chiral spin liquid phase MZMs can appear exhibiting a non-local correlation and  $Z_2$  fluxes binding them obey non-Abelian statistics, in principle. It is expected to exploit the composite particles for topological quantum computation. It is difficult, however, to introduce and control the composites in the ground state of the pure Kitaev model since they are thermal excitations. To avoid the difficulty, we focus on point vacancies in the system. It is well known that each vacancy binds  $Z_2$  flux in the ground state, or the bound-flux sector [2], while MZMs strongly trapped in them are not yet reported.

In this study, we reveal the importance of localized Majorana fermions caused by vacancies, which have not been properly taken into account in previous studies. In the Kitaev's notation, a spin operator at  $j$ -site,  $S_j^\gamma$  ( $\gamma = x, y, z$ ), is represented as  $S_j^\gamma = ib_j^\gamma c_j / 2$ , using an itinerant Majorana fermion operator  $c_j$  and a localized Majorana fermion opera-

tor  $b_j^\gamma$  (Fig. 1). The former behaves as a free Majorana fermion described as a tight-binding model while the latter forms a  $Z_2$  gauge field with the other localized Majorana fermion from the nearest site on each bond. Then, if a vacancy exists, the localized Majorana fermion from the nearest site of the vacancy site loses the partner and it can couple with itinerant Majorana fermions, as shown in Fig. 1, when an external magnetic field is applied. This non-trivial Majorana hopping term, or b-c hopping term, contributes to realizing MZMs bound in  $Z_2$  fluxes that should be naturally found in the bound-flux sector.

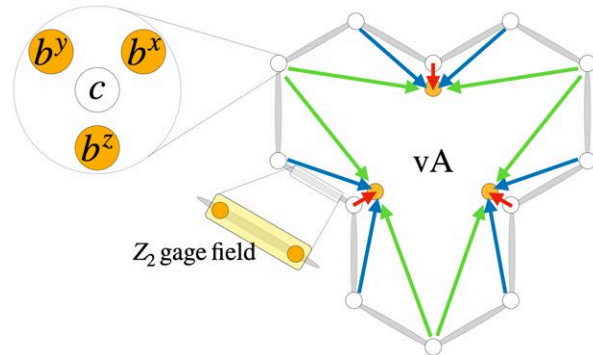


Figure 1: Majorana fermions for each spin and nontrivial Majorana hoppings between  $b_j^\gamma$  and  $c_k$  around a vacancy vA, represented as arrows.

The effective Majorana Hamiltonian  $H_{\text{eff}}$  for the Kitaev model with vacancies, which are spatially well-separated, works well to host MZMs. We assume two vacancies, vA and vB, for simplicity and the direction of a magnetic field parallel to the in-plane a-axis. At nonzero

magnetic fields, a pair of MZMs appears in the bulk gap and is stable against an increase in a magnetic field strength unless the bound-flux ground state is valid. This property is not confirmed without b-c Majorana hopping terms: the Majorana gap grows as increasing the strength whereas pseudo-MZMs [3] disappear rapidly to form the bulk gap. Moreover, it is discovered that more than 99% of the real-space amplitudes of MZMs are on the localized Majorana fermions, which implies that they are strongly trapped in  $Z_2$  fluxes in the ground state.

To approach a pair of MZMs by a physical observable using a non-local property, we consider a non-local spin correlation between the nearest sites of each vacancy, say  $j_A$  and  $j_B$  site. Our interest is written as below at inverse temperature  $\beta$ ,

$$\langle S_{j_A}^z(t) S_{j_B}^z(0) \rangle \equiv \frac{\text{Tr} \left[ P_F S_{j_A}^z(t) S_{j_B}^z(0) e^{-\beta H_{\text{eff}}} \right]}{\text{Tr} \left[ P_F e^{-\beta H_{\text{eff}}} \right]}, \quad (1)$$

where  $P_F$  is a projection operator to the physical subspace. Especially the

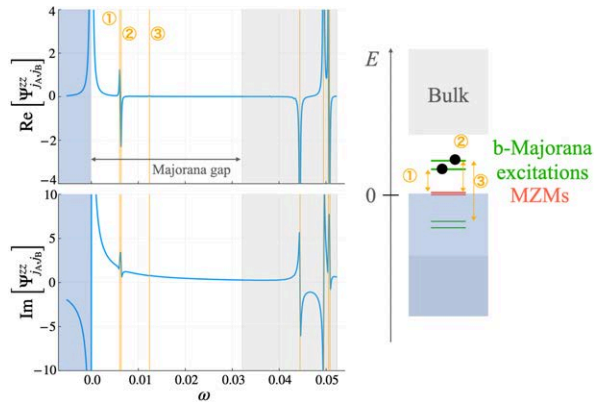


Figure 2: The structure factor of a non-local spin-spin correlation and the Majorana spectrum structure.

Fourier-transformed dynamical structure factor  $\Psi_{j_A j_B}^{zz}(\omega) \equiv \int_0^\infty e^{i(\omega+i\delta)t} \langle S_{j_A}^z(t) S_{j_B}^z(0) \rangle$  clearly reveals the contribution from MZMs and b-Majorana excitations inside the bulk gap

as shown in Fig. 2. Indeed, the structure factor in the zero-flux sector differs from the one in the bound-flux ground state in a point that the signal comes from b-Majorana excitations shift to a higher  $\omega$  region, very close to the Majorana bulk gap, which implies the absence of MZMs.

In summary, non-Abelian anyons composed of MZMs and  $Z_2$  fluxes, both of which are trapped in vacancies, can stably exist in the ground state of the vacancy-induced Kitaev model with a magnetic field. They exhibit the non-local spin-spin correlation in a chiral *spin liquid* phase, and this system may become the new platform for topological quantum computation.

## References

- [1] A. Kitaev, Ann. Phys. **321** (2006) 2.
- [2] A. J. Willans et al., Phys. Rev. Lett. **104** (2010) 237203.
- [3] W.-H. Kao and N. B. Perkins, Ann. Phys. **435** (2021) 168506.

# Discrete time crystals in solids

Tatsuhiko Ikeda

*Institute for Solid State Physics, University of Tokyo  
Kashiwa-no-ha, Kashiwa, Chiba 277-8581*

We have studied a discrete time crystal (DTC) in solid-state materials using Supercomputer System B at the ISSP. This year, a paper on this project was published [1]. We will report this project below.

A DTC is an exotic nonequilibrium phase in periodically driven dissipative quantum systems that breaks the discrete time translation symmetry. The DTC had been well studied and experimentally demonstrated in artificial quantum systems without dissipation, such as trapped ions, NV centers in diamond, and quantum computers. However, it had not been explored in natural materials, like solids, with dissipation. Nonetheless, if we create the DTC in natural materials, it could offer a new possibility of time crystals in material science.

In this study, we have investigated the DTC in solid-state materials. To uncover the mechanism and properties of the DTC in solids, we have considered a periodically driven quantum Ising model with dissipation using the Floquet-Redfield equation that describes a periodically driven quantum system subject to dissipation. The Floquet-Redfield equation is much harder to solve than the usual Schrödinger equation because we need to treat a  $D \times D$  density matrix rather than a  $D$ -dimensional wave function in the Floquet-Redfield equation ( $D$  is the Hilbert space dimension). Therefore, in this study, we have employed the mean-field theory and numerically solved the DTC order parameter self-consistently.

Performing a massive numerical calculation with the supercomputer, we have obtained

the phase diagram of the DTC in solids (see Fig. 1). This phase diagram highlights a non-trivial behavior that the separate two DTC regions appear. Also, we have shown that this DTC is robust against any perturbation. We believe that these results pave the way for a new research field of time crystals in material science.

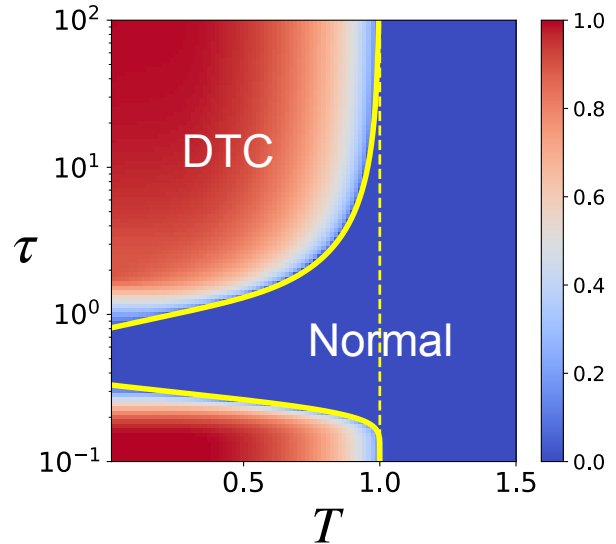


Figure 1: Phase diagram of the DTC in solids. The horizontal (vertical) axis denotes the temperature of the bath (the period of the Hamiltonian).

## References

- [1] K Chinzei and TN Ikeda: Phys. Rev. Research **4**, 023025 (2022).

# Interaction-induced quantum spin Hall state in the Dirac electron system $\alpha$ -(BEDT-TSeF) $_2$ I $_3$

Akito KOBAYASHI

*Department of Physics, Nagoya University**Nagoya 464-8602*

We have constructed extended-Hubbard model using first-principles calculations to deal with spin-orbit and non-local repulsive interactions and have shown that an interaction-induced quantum spin Hall (QSH) state is stabilized, focusing on the recently-discovered candidate topological insulator  $\alpha$ -(BEDT-TSeF) $_2$ I $_3$  having two-dimensional charge-neutral Dirac cones.[1, 2, 3, 4] In the absence of repulsive interactions, a topological insulator characterized by a nonzero spin Chern number appears by the spin-orbit coupling. By considering up to next-nearest neighbor repulsions at Hartree-Fock level, the intrinsic spin-orbit gap is found to grow and a QSH state appears that has both a nonzero spin Chern number and order parameter as shown in Fig. 1. The loops  $\phi_i$  shown in Fig. 1 represents the spin current flowing between BEDT-TSeF molecules. The spin currents between next-nearest neighboring molecules also exist, but they are omitted in Fig. 1 for simplicity. These spin currents increase at low temperatures below 50 K and widen the gap. Transport coefficients and spin susceptibility have been calculated and found to be consistent with most of the experimental findings, including the metal-to-insulator crossover occurring at  $\sim 50$  K as well as the Berry phase change from 0 to  $\pi$  under hydrostatic pressure. We argue that such a QSH state does not necessitate a sizeable spin-orbit interaction to generate a large insulating gap, which is highly advantageous for the search of novel topological phases in generic

materials having small spin-orbit coupling.

## References

- [1] S. Kitou, et al., Phys. Rev. B 103, 035135 (2021).
- [2] T. Tsumuraya et al., Eur. Phys. J. B, 94, 17 (2021).
- [3] Y. Suzumura et al., JPSJ 90, 124707 (2021).
- [4] D. Ohki, K. Yoshimi, and A. Kobayashi, arXiv:2110.05010

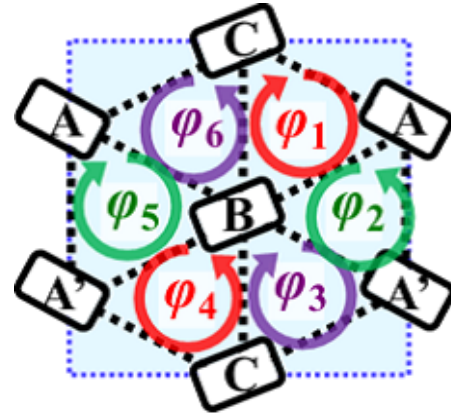


Figure 1: Interaction-induced quantum spin Hall state in  $\alpha$ -(BEDT-TSeF) $_2$ I $_3$ .

# Study of cuprate high-temperature superconductors using a four-band $d$ - $p$ model

Hiroshi WATANABE

*Research Organization of Science and Technology, Ritsumeikan University  
1-1-1 Noji-Higashi, Kusatsu-shi, Shiga 525-8577*

The discovery of superconductivity in cuprates [1] has brought about the significant progress in strongly-correlated electron systems. However, we have not yet reached a unified understanding of their properties, including their material dependence of the superconducting transition temperature  $T_c$ . Recent development of theories and experiments sheds light on the importance of the orbital degree of freedom in cuprates [2, 3]. To obtain the unified description of cuprate high-temperature superconductors, we study the four-band  $d$ - $p$  model that properly includes the orbital degree of freedom [4]. We construct the tight-binding model for  $\text{La}_2\text{CuO}_4$  and  $\text{HgBa}_2\text{CuO}_4$  systems based on the first-principles calculation and examine the effect of Coulomb interactions with the variational Monte Carlo (VMC) method. The Gutzwiller-Jastrow type wave function is used for the VMC trial wave function. The system size for the calculation is  $N=24 \times 24=576$  unit cells (and thus  $576 \times 4=2304$  orbitals in total), which is large enough to avoid finite size effects.

The superconducting correlation function  $P^{dd}$  vs hole doping rate  $x$  for the  $\text{La}_2\text{CuO}_4$  system is shown in Fig. 1. At  $x = 0$ , the system is insulating and the superconductivity is completely suppressed:  $P^{dd} = 0$ . As  $x$  increases, mobile carriers are introduced into the system and the mobility of the Cooper pair increases. On the other hand, the strength of the  $d$ - $d$  pairing itself is reduced by doping because the electron correlation is also re-

duced. The balance between these two factors results in the dome-shaped behavior of  $P^{dd}$ . The  $U_d/t_1$  dependence of  $P^{dd}$  can be also understood with this picture. We consider that  $U_d/t_1 \sim 8$  is a realistic value for the  $\text{La}_2\text{CuO}_4$  system. For the  $\text{HgBa}_2\text{CuO}_4$  system, while the dome-shaped behavior is observed for  $U_d/t_1 = 7$  and 8,  $P^{dd}$  monotonically decreases with  $x$  for  $U_d/t_1 = 6$ . This is because the system is metallic for  $U_d/t_1 = 6$  and the picture of “doped Mott insulator” is no longer valid. It results from the smaller  $\Delta_{dp}$  in the  $\text{HgBa}_2\text{CuO}_4$  system that leads to the weaker electron correlation compared with the  $\text{La}_2\text{CuO}_4$  system. The difference between two systems are well described in our four-band  $d$ - $p$  model.

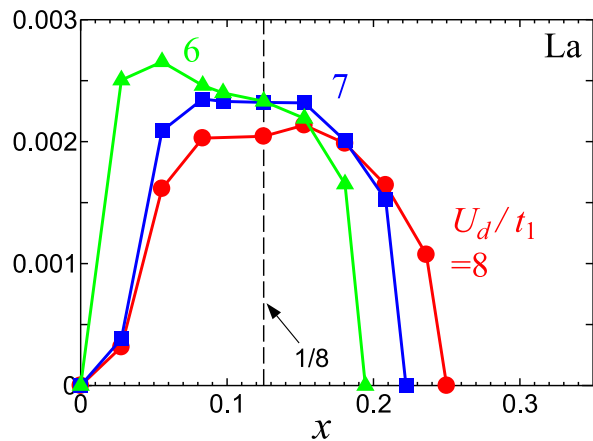


Figure 1: Superconducting correlation function  $P^{dd}$  vs hole doping rate  $x$  for the  $\text{La}_2\text{CuO}_4$  system.

## References

- [1] J. G. Bednorz and K. A. Muller, *Z. Phys. B* **64**, 189 (1986).
- [2] H. Sakakibara et al., *Phys. Rev. Lett.* **105**, 057003 (2010).
- [3] C. E. Matt et al., *Nat. Commun.* **9**, 972 (2018).
- [4] H. Watanabe et al., *Phys. Rev. Research* **3**, 033157 (2021).

# Superconductivity in correlated electron systems

Takashi YANAGISAWA

*National Institute of Advanced Industrial Science and Technology (AIST)  
1-1-1 Umezono, Tsukuba 305-8568*

## 1 Introduction

Our computations are mainly based on the optimized variational Monte Carlo method[1]. We also employ the Gutzwiller-Jastrow wave function where the doublon-holon correlation is taken into account. We have investigated the ground-state phase diagram of the two-dimensional Hubbard model and the two-dimensional d-p model. We performed parallel computation in Monte Carlo calculations. In order to reduce statistical errors, we carried out  $\sim 500$  parallel calculations. Parallel computing is very important to reduce Monte Carlo statistical errors.

The many-body wave function is written in the form  $\psi^{(1)} = \exp(-\lambda K)P_G\psi_0$ , where  $K$  denotes the kinetic energy part (non-interacting part) of the Hamiltonian and  $P_G = P_G(g)$  is the Gutzwiller operator to control the double occupancy with the variational parameter  $g$ .  $\psi_0$  indicates a trial wave function which is usually taken as the Fermi sea, the BCS wave function or the state with some magnetic (or charge) orders. We can improve the wave function systematically by multiplying by operators  $P_G$  and  $e^{-\lambda K}$  repeatedly. We can consider  $\psi^{(2)} = \exp(-\lambda' K)P_G(g')\psi^{(1)}$  for different variational parameters  $\lambda'$  and  $g'$ . This wave function is a very good many-body wave function because the ground-state energy is lowered greatly and the ground-state energy is lower than those that are evaluated by any other wave functions. We also employ the Jastrow-type wave function which is written as  $\psi_J = P_G P_Q P_J \psi_0$  where  $P_J$  indicates a nearest-neighbor number correlation operator and  $P_Q$  controls the nearest-neighbor doublon-holon correlation.

## 2 Why does the pairing state become stable?

We have shown that the superconducting phase exists in the strongly correlated region of electronic models[2]. We investigated kinetic-energy effect in superconductivity in the strongly correlated phase of the two-dimensional Hubbard model. Let us examine why the superconducting state becomes stable in the strongly correlated region. The Gutzwiller-BCS state is stabilized as a potential energy driven superconductivity because the Coulomb interaction energy is lowered while the kinetic energy increases in this state. In contrast, we showed that in the  $\psi_\lambda$ -BCS wave function  $\psi_{\lambda-BCS} = e^{-\lambda K}P_G\psi_{BCS}$ , the Coulomb energy increases and instead the kinetic energy is lowered in the strongly correlated phase where the Coulomb repulsive interaction  $U$  is large. The correlated superconducting state is realized as a kinetic energy driven pairing state and this indicates the enhancement of superconductivity due to kinetic-energy effect.

We estimate the kinetic energy in the superconducting state  $\psi_{\lambda-BCS}$ [3]. We define the SC condensation energy  $\Delta E_{sc}$  as a sum of two contributions  $\Delta E_{kin-sc}$  and  $\Delta E_{U-sc}$ :

$$\begin{aligned}\Delta E_{sc} &= E(\Delta = 0) - E(\Delta = \Delta_{opt}), \\ \Delta E_{kin-sc} &= E_{kin}(\Delta = 0) - E_{kin}(\Delta = \Delta_{opt}), \\ \Delta E_{U-sc} &= E_U(\Delta = 0) - E_U(\Delta = \Delta_{opt}),\end{aligned}$$

where  $\Delta = \Delta_{sc}$  is the SC order parameter and  $\Delta_{opt}$  is the optimized value which gives the energy minimum. We have

$$\Delta E_{sc} = \Delta E_{kin-sc} + \Delta E_{U-sc}. \quad (1)$$

The kinetic energy in  $\psi_{\lambda-BCS}$  is lower than the kinetic energy in the normal state  $\psi_\lambda$ . The

Coulomb energy expectation value increases as  $\Delta_{sc}$  increases. The results show

$$\Delta E_{kin-sc} > 0, \quad \Delta E_{U-sc} < 0, \quad (2)$$

for  $\psi_{\lambda-BCS}$  with  $U = 18t$  and the hole density  $x = 0.12$ .

### 3 Kinetic energy enhancement of superconductivity

We define the difference of the kinetic energy as

$$\Delta E_{kin} = E_{kin}(\psi_G) - E_{kin}(\psi_\lambda), \quad (3)$$

where  $E_{kin}(\psi_G)$  and  $E_{kin}(\psi_\lambda)$  indicate the kinetic energy for  $\psi_G$  and  $\psi_\lambda$ , respectively. We can write  $\Delta E_{kin} = E_{kin}(\lambda = 0) - E_{kin}(\lambda)$  for the optimized value of  $\lambda$ .  $\Delta E_{kin}$  has the close relation with the SC condensation energy  $\Delta E_{sc}$  and its kinetic part  $\Delta E_{kin-sc}$ .

We show  $\Delta E_{kin}/N$  in Fig. 1 for  $x = 0.12$  where  $x$  is the hole doping rate. The Coulomb energy  $E_U/N$  and the superconducting condensation energy  $\Delta E_{sc}/N$  are also shown in Fig. 1.  $\Delta E_{kin}$  begins to increase after the Coulomb energy  $E_U$  reaches the peak when  $U \approx 8t$ . The  $y$  axis on the right shows  $\Delta E_{kin-sc}/N$  in Fig. 1.  $\Delta E_{kin-sc}$  shows a similar behavior to  $\Delta E_{kin}$ .  $\Delta E_{kin-sc}$  may change sign as a function of  $U$ , which is consistent with the analysis for  $\text{Bi}_2\text{Sr}_2\text{CaCu}_2\text{O}_{8+\delta}$ [4]. This shows the kinetic energy enhancement of superconductivity.

### 4 Summary

We examined the kinetic energy effect in SC states. The Gutzwiller-BCS state is the potential energy driven SC state, because the SC condensation energy comes from the Coulomb interaction energy. This is the same as the original BCS state where the superconductivity appears due to the attractive interaction. We evaluated the kinetic energy in the improved SC state ( $\psi_{\lambda-BCS}$ ) to find that the kinetic energy gain stabilizes SC state while the expectation value of Coulomb interaction energy increases. This indicates that superconductivity is enhanced due to the kinetic energy effect.

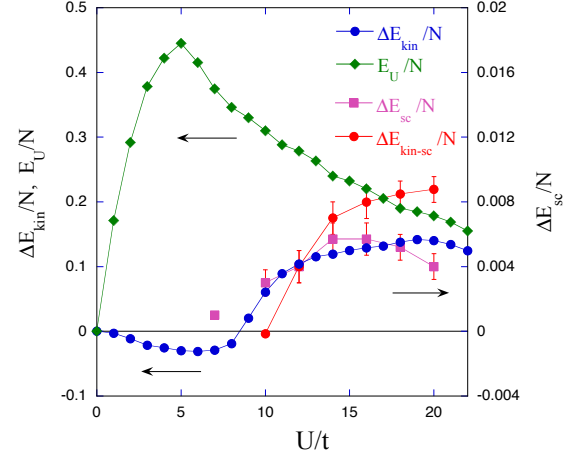


Figure 1: Kinetic-energy difference  $\Delta E_{kin}/N$  and the kinetic-energy gain  $\Delta E_{kin-sc}/N$  in the superconducting state  $\psi_{\lambda-BCS}$  as a function of  $U$  on a  $10 \times 10$  lattice where  $N_e = 88$  and  $t' = 0$ . The Coulomb energy  $E_U/N$  for  $\psi_\lambda$  and the condensation energy  $\Delta E_{sc}$  are also shown. We use the periodic boundary condition in one direction and antiperiodic one in the other direction. The  $y$  axis on the right shows the superconducting condensation energy  $\Delta E_{sc}$  and the kinetic condensation energy  $\Delta E_{kin-sc}/N$  for  $\psi_\lambda$ .

### References

- [1] T. Yanagisawa et al., J. Phys. Soc. Jpn. 67, 3867 (1998).  
T. Yanagisawa, Phys. Rev. B75, 224503 (2007) (arXiv: 0707.1929).
- [2] T. Yanagisawa, J. Phys. Soc. Jpn. 85, 114707 (2016).  
T. Yanagisawa, J. Phys. Soc. Jpn. 88, 054702 (2019).  
T. Yanagisawa, Condensed Matter 4, 57 (2019).
- [3] T. Yanagisawa, Phys. Lett. A403, 127382 (2021).  
T. Yanagisawa et al., EPL 134, 27004 (2021).
- [4] G. Deutscher, A. F. Santander-Syro, N. Bontemps: Phys. Rev. B 72, 092504 (2005).

# Photoinduced nonequilibrium dynamics in correlated electron systems

Atsushi ONO

*Department of Physics, Tohoku University,  
Sendai 980-8578*

Antiferromagnets are promising for spintronics applications owing to their robustness against a perturbative field and to a higher energy scale compared with that of ferromagnets. Recently, a current-induced staggered torque, called Néel spin-orbit torque (NSOT), has been recognized as an efficient mechanism that rotates the Néel vector in antiferromagnets. However, since most of the previous studies considered the electrical switching of the antiferromagnets, it is not fully understood whether and how the NSOT is generated by optical pulses.

We have studied the real-time dynamics induced by a static electric field and a terahertz electric-field pulse [1]. We considered a minimal tight-binding model of antiferromagnetic Dirac semimetals, where a nonsymmorphic symmetry associated with the direction of the Néel vector protects the crossing of doubly degenerated energy bands, i.e., Dirac points. The time evolution is governed by the Landau–Lifshitz–Gilbert equation for the localized moments and the von Neumann equation for the itinerant electrons. We solved these coupled equations by using the ISSP supercomputer system.

Figure 1 shows the real-time dynamics induced by a mono-cycle electric-field pulse. We found that the Néel vector rotates in a picosecond timescale, depending on the amplitude and polarization of light, and the Néel-vector rotation accompanies the change in the energy gap at the Dirac points. Our analy-

sis revealed that the Néel vector is canted by optical NSOT and then rotated by a magnetic-anisotropy torque. We also showed that in this system a magneto-optical effect can be used to observe the direction of the Néel vector in real time.

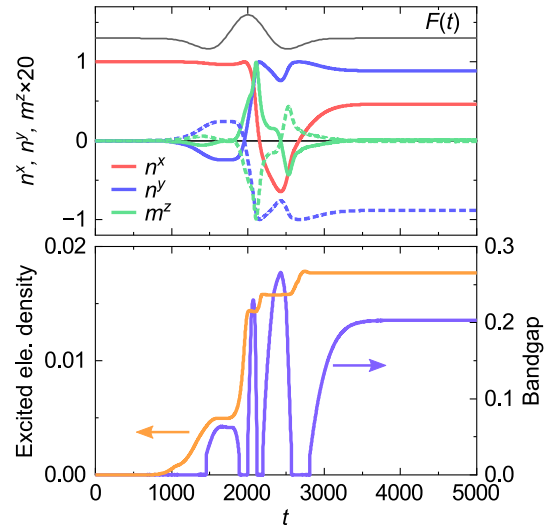


Figure 1: Time evolution of the Néel vector  $\mathbf{n}$ , uniform magnetization  $\mathbf{m}$ , excited electron density, and bandgap [1]. A mono-cycle electric-field pulse  $F(t)$  is applied.

## References

- [1] A. Ono and S. Ishihara, *npj Comput. Mater.* **7**, 171 (2021).